Magnetic Fields from Low-Mass Stars to Brown Dwarfs

Julien Morin

MAGNETIC FIELDS FROM LOW MASS STARS TO BROWN DWARFS

J. Morin[1, 2]

Abstract. Magnetic fields have been detected on stars across the H-R diagram and substellar objects either directly by their effect on the formation of spectral lines, or through the activity phenomena they power which can be observed across a large part of the electromagnetic spectrum. Stars show a very wide variety of magnetic properties in terms of strength, geometry or variability. Cool stars generate their magnetic fields by dynamo effect, and their properties appear to correlate — to some extent — with stellar parameters such as mass, rotation and age. With the improvements of instrumentation and data analysis techniques, magnetic fields can now be detected and studied down to the domain of very-low-mass stars and brown dwarfs, triggering new theoretical works aimed, in particular, at modelling dynamo action in these objects. After a brief discussion on the importance of magnetic field in stellar physics, the basics of dynamo theory and magnetic field measurements are presented. The main results stemming from observational and theoretical studies of magnetism are then detailed in two parts: the fully-convective transition, and the very-low mass stars and brown dwarfs domain.

1 Introduction

Magnetic fields have often been neglected in early astrophysical theories, both for simplicity and lack of observational data. However, recent advances point out the crucial role of magnetic fields in many aspects of stellar physics; besides the number of stellar magnetic field measurements is constantly growing and the coverage of the H-R diagram constantly improving (Donati and Landstreet 2009; Reiners 2012). Magnetic fields are particularly important during the formation and early evolution

[1] Dublin Institute for Advanced Studies, School of Cosmic Physics, 31 Fitzwilliam Place, Dublin 2, Ireland

[2] Institut für Astrophysik, Georg-August-Universität, Friedrich-Hund-Platz 1, D-37077 Göttingen, Germany; e-mail: `jmorin@gwdg.de`

of stars: for instance they can oppose the gravitational collapse of molecular clouds (see chapter by P. Hennebelle, this book), the launching and confinement of bipolar jets observed on protostars are MHD phenomena (Tsinganos et al. 2009), and matter accreted from the circumstellar disc onto a T Tauri star is thought to be channelled along magnetic fields lines (Bouvier et al. 2007). Magnetic fields are also know to play a key role in the rotational evolution of low-mass stars, indeed most of the phenomena which drive this evolution (*e.g.,* star-disc coupling, stellar winds) involve magnetic fields (Bouvier 2009). An additional issue that has emerged since the discovery of the first exoplanet (Mayor and Queloz 1995) has been the impact stellar of magnetic fields and activity on the formation, evolution, and habitability of planetary systems, as well as on the detection of planets orbiting around active stars (see chapter by X. Bonfils, this book). All these topics are quite relevant to low mass stars and brown dwarfs, as demonstrated by recent studies such as the detection of outflows on substellar objects (Whelan et al. 2005), the observational and theoretical works addressing the rotational evolution of M dwarfs (Irwin et al. 2011; Reiners and Mohanty 2012), and the ongoing or planned planet-search programs targeting M dwarfs (Bonfils et al. 2011). Moreover, since some of them host very strong magnetic fields, low mass stars and brown dwarfs are particularly interesting laboratories to study the effect magnetism on stellar internal structure (Chabrier et al. 2007). Last but not least, low mass stars and brown dwarfs appear as a vital link to build a consistent picture of dynamo action in astrophysical bodies from planets to solar-type stars (Christensen et al. 2009).

2   Dynamo action in cool stars

A fundamental difference exists among stars regarding the origin of the magnetic fields that are detected in their outer atmosphere. On the one hand, in some stars with outer radiative zones or in compact objects, simple and steady magnetic fields are observed. They are generally thought to be fossil fields[1], *i.e.* to be the remnant of a field generated at an earlier phase of their evolution. On the other hand, cool stars (*i.e.* spectral types later than mid-F) as well as brown dwarfs possess an outer convective envelope where the magnetic diffusivity is strongly enhanced by fluid motions (*e.g.,* Rüdiger et al. 2011), resulting in field decay times of the order of a decade. The very existence of significant magnetic fields on cool stars with ages of the order of a Gyr, as well as their dynamic nature (in particular the existence of magnetic cycles) point out that magnetic fields have to be generated in these objects, namely by dynamo action.

2.1   A few words of history

Hale (1908) first measured strong magnetic fields (several kilogauss) in sunspots. This observation revealed at the same time the existence of the solar magnetic field

---

[1] Although the possibility for magnetic field generation in stellar radiative zones is a debated topic (*e.g.,* Braithwaite and Spruit 2004)
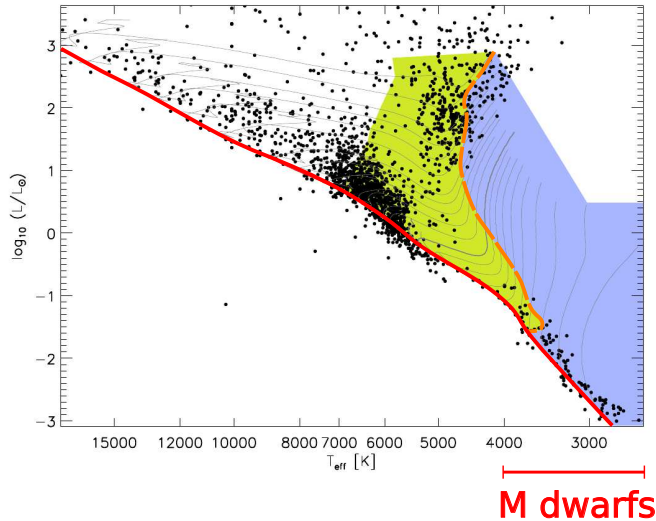
Figure 1: Hertzsprung–Russel diagram with evolutionary tracks from Siess et al. (2000). Cool stars are located in the green (partly convective) and blue (fully convective) regions. The main sequence is depicted as a red solid line and the fully convective limit as an orange dashed line. M dwarfs are located at the cool end of the main sequence. Even cooler L, T and Y dwarfs (*i.e.* brown dwarfs) are not represented here. Adapted from Reiners (2008).

as well as its cyclic nature, according with previous knowledge about sunspots: the 11-yr cyclic variation of their number (Schwabe 1844), and their migration in latitude during the cycle (the "butterfly diagram", Maunder 1904). These results were later complemented by the discovery of the polarity law of sunspots making the magnetic cycle 22 yr long (Hale et al. 1919). In addition to sunspots, a weak (of the order of 1 G) large-scale component of the solar magnetic field which follows the the same 22-yr cycle is also observed (Babcock and Babcock 1955; Babcock 1961). Both the relative importance of the dipole and quadrupole components, as well as their tilt angle with respect to the solar rotation axis were shown to evolve during the solar cycle (Sanderson et al. 2003). Although the strong magnetic fields associated with sunspots and the large-scale solar field are likely the two features that receive the most attention for models of the solar cycle, a whole "zoo" of solar magnetic features exists, the reader is referred to Solanki et al. (2006).

Larmor (1919) first proposed that the solar magnetic field could be induced by motions of an electrically conducting fluid. He also pointed out the possible role of differential rotation to generate a strong ordered azimuthal field deep inside the Sun, such as mentioned by Hale et al. (1919) to explain the properties of sunspots. This was the first step toward the concept of solar magnetism powered by dynamo action, *i.e.* a mechanism able to convert kinetic energy of plasma motions into magnetic energy in a self-sustained manner. However this idea was

severely hampered by Cowling (1933)'s anti-dynamo theorem which states that a purely axisymmetric field cannot be sustained by dynamo action. Elsasser (1946)[2] then introduced the poloidal–toroidal decomposition of the magnetic field (see Appendix A) and formalized Larmor's idea on the role of differential rotation by showing that it could transform a poloidal field into a stronger toroidal one, this is now referred to as the Ω-effect. He also demonstrated that differential rotation alone was not enough to sustain a dynamo (toroidal theorem), another mechanism is indeed required to regenerate a poloidal component from the toroidal field.

A first solution was initiated by Parker (1955): convective motions in the solar envelope are deflected by the Coriolis force, this twists the field lines in a systematic way and allows the regeneration of poloidal field from toroidal field. The combination of this effect with the aforementioned Ω-effect constitutes the first model of an hydromagnetic self-sustained dynamo. Steenbeck et al. (1966) then introduced the mean-field theory and the α-effect which turned out to be closely related to Parker's concept of cyclonic convection.

2.2   A few words of mean-field theory

The dynamo effect consists in generating and sustaining a magnetic field from the motion of an electrically conducting fluid, *i.e.* converting kinetic energy into magnetic energy. Dynamos are thought to operate in many astrophysical objects from telluric and gaseous planets, to stars and galaxies. The main concepts as well some vocabulary often encountered in the literature are presented here. For a more detailed view of dynamo theory, the reader is referred to the following reviews and books: Ossendrijver (2003); Rüdiger and Hollerbach (2004); Brandenburg and Subramanian (2005); Dormy and Soward (2007); Charbonneau (2010). The fundamental equation for this problem is the induction equation, it can be derived from the Maxwell–Faraday and Maxwell–Ampère equations combined with the generalized Ohm's law[3]:

$$\frac{\partial \mathbf{B}}{\partial t} = \nabla \times (\mathbf{u} \times \mathbf{B} - \eta \nabla \times \mathbf{B}) = \underbrace{\nabla \times (\mathbf{u} \times \mathbf{B})}_{induction} + \underbrace{\eta \mathbf{\Delta B}}_{dissipation}, \qquad (2.1)$$

where $\mathbf{B}$ and $\mathbf{u}$ are respectively the magnetic field and fluid velocity vectors, and η is the magnetic diffusivity. The ratio between the two terms of RHS of the induction equation can be approximated by the magnetic Reynolds number:

$$\mathrm{Rm} = \frac{\mathrm{induction}}{\mathrm{diffusion}} = \frac{\frac{u_0 B_0}{L}}{\frac{\eta B_0}{L^2}} = \frac{u_0 L}{\eta}, \qquad (2.2)$$

where u_0, B_0 and L are characteristic velocity, magnetic field modulus and length scale. For dynamo action to be possible Rm must therefore necessarily be larger

---

[2]Elsasser's work was originally mostly focused on the geodynamo problem, but his formalism was also rapidly used for the solar dynamo.

[3]As opposed to Maxwell's equation and Ohm's law, the induction equation does not depend on the choice of SI or CGS units

than unity, although this condition is not sufficient. We note that in the convection zones of cool stars estimates show that this condition is satisfied (*e.g.,* Brandenburg and Subramanian 2005, table 1). Solar and stellar physicists are generally interested in large-scale dynamos, *i.e.* which generate magnetic field on spatial scales larger than that of the convection and can explain the properties of magnetic cycles[4]. Not any flow can act as a large-scale dynamo, in particular a number of anti-dynamo theorem (*cf.* Sec. 2.1) indicate that some specific properties are required.

In order to fully address the dynamo problem, one has to consider, in addition to the induction equation, the $\nabla \cdot \mathbf{B} = 0$ Maxwell's equation, as well as an equation of state and the Navier-Stokes equations to describe the fluid motion. We also note that according to the anti-dynamo theorems, the dynamo problem is intrinsically 3-D and cannot be addressed by considering 2-D flow and magnetic field. The mean field approach has been developed by Steenbeck et al. (1966); Steenbeck and Krause (1969a,b)[5] in order to allow for a simplified treatment of the dynamo problem, this theoretical framework remains important in our understanding of the solar dynamo as well as in the vocabulary. This is a kinetic approach, *i.e.* the induction equation is solved for a given flow, the feedback of the Lorentz force on the fluid motion is not considered. Its specificity consists in decomposing both the magnetic and velocity field into the sum of a mean and a fluctuating components, generally understood as the axisymmetric and non-axisymmetric parts, though any averaging operator for which the Reynolds rules apply can be used (see *e.g.,* Rädler and Rheinhardt 2007). Let $\langle \cdot \rangle$ be this averaging operator:

$$\mathbf{x} = \langle \mathbf{x} \rangle + \mathbf{x}', \tag{2.3}$$

where $\mathbf{x}$ can be either $\mathbf{u}$ or $\mathbf{B}$, and $\mathbf{x}'$ is the fluctuating component. By introducing this decomposition into equation (2.1), one gets:

$$\frac{\partial \langle \mathbf{B} \rangle}{\partial t} = \nabla \times \left(\langle \mathbf{u} \rangle \times \langle \mathbf{B} \rangle + \langle \mathbf{u}' \times \mathbf{B}' \rangle - \eta \nabla \times \langle \mathbf{B} \rangle \right). \tag{2.4}$$

The main difference with (2.1) is the presence of the term $\langle \mathbf{u}' \times \mathbf{B}' \rangle$ which is referred to as the turbulent electromotive force. It is the presence of the fluctuating fields in the source term of the induction equation for the mean magnetic field which can circumvent Cowling's theorem. Up to this point no approximation has been made, but in order to solve Eq. (2.4), a closure equation linking the fluctuating quantities to the mean magnetic field is required, this is detailed by *e.g.,* Rädler and Rheinhardt (2007). The simplest approach assumes *(i)* a clear scale separation between and the mean and fluctuating components and *(ii)* that the fluctuating velocity field corresponds to homogeneous and isotropic turbulence,

---

[4]Although a turbulent or small-scale dynamo likely coexists (Durney et al. 1993; Dorch and Ludwig 2002; Vögler and Schüssler 2007)

[5]These papers were originally published in German and later translated in English by Moffatt (1970); Roberts and Stix (1971)

the turbulent EMF is then expressed as:

$$\langle \mathbf{u}' \times \mathbf{B}' \rangle = \alpha \langle \mathbf{B} \rangle - \beta \nabla \times \langle \mathbf{B} \rangle. \tag{2.5}$$

By substituting this expression for the turbulent EMF and introducing the poloidal-toroidal decomposition (A.2) into equation (2.4) one gets the evolution equations for the mean poloidal and toroidal field respectively:

$$\begin{cases} \dfrac{\partial A}{\partial t} + \dfrac{1}{s}(\mathbf{u}_{\text{pol}} \cdot \nabla)(sA) = & \alpha B \quad + (\eta + \beta)\nabla_1^2 A \\ \dfrac{\partial B}{\partial t} + s(\mathbf{u}_{\text{pol}} \cdot \nabla)(\dfrac{B}{s}) = \underbrace{s\mathbf{B}_{\text{pol}} \cdot \nabla\Omega}_{\Omega\text{-effect}} \underbrace{-\alpha\nabla_1^2 A}_{\alpha\text{-effect}} + \underbrace{(\eta + \beta)\nabla_1^2 B}_{dissipation}, \end{cases} \tag{2.6}$$

$$\text{with } s = r\sin\theta \ ; \ \nabla_1^2 = \left(\Delta - \dfrac{1}{s^2}\right) \ ; \ \mathbf{B}_{\text{pol}} = \nabla \times (A\mathbf{e}_\phi), \tag{2.7}$$

where spherical coordinates (r, θ, ϕ) are used and $\mathbf{B}_{\text{pol}}$ is the poloidal component of the mean magnetic field. A few comments can be made on equation (2.6):

- The α-effect is related to the mean kinetic helicity of the turbulent flow[6], thus representing in a more formalized way Parker's idea of convective motions systematically deflected and twisted by the Coriolis force.

- The β-effect on its side is related to the kinetic energy of the turbulent flow and acts as an enhanced dissipation. In stellar convection zones, estimates show that this turbulent diffusivity is higher than the intrinsic diffusivity of the plasma by several order of magnitudes.

- The Ω-effect can only produce toroidal field from a poloidal component, and therefore a dynamo cannot rely on this effect alone, the alpha effect is necessary to regenerate a poloidal component of the field. On the opposite, as the α-effect is present as a source term in both the poloidal and the toroidal induction equations, a dynamo can rely on this effect alone.

- The Ω-effect depends on differential rotation, solid-body rotation is related to the α-effect through the Coriolis force that generates kinetic helicity.

- Dynamos in which toroidal field generation is predominantly due to the α-effect (Ω) are called α^2 ($\alpha\Omega$), and the intermediate case where both terms have similar order of magnitude is sometimes referred to as $\alpha^2\Omega$.

---

[6]The kinetic helicity $\langle \mathbf{u} \cdot (\nabla \times \mathbf{u}) \rangle$ characterize the fact that the fluid has both a rotation movement and a translation collinear with the rotation axis, as would be the case for a movement along a helix.

2.3 Later developments and the role of the tachocline

An important success of the mean-field theory with parametrized α-effect resides in that $\alpha\Omega$ dynamos can exhibit cyclic solutions that can be related to the solar cycle (Steenbeck and Krause 1969a). However, additional issues have emerged which have questioned the mean-field approach and the validity of the results obtained, for a critical detailed critical view see Spruit (2011). First, the generation of the very strong toroidal fields required to explain the observed properties of sunspots appeared incompatible with the magnetic buoyancy instability (Parker 1975). Secondly, the mechanism that generates poloidal magnetic field from a toroidal component is still debated, and alternatives to and improvements of the α-effect are proposed, such as the Babcock-Leighton mechanism (Babcock 1961; Leighton 1969), or generation mechanisms based on MHD instabilities (see the discussion on poloidal field generation mechanisms in Charbonneau 2010). Third, there are intrinsic limitations of the mean-field kinematic approach itself which does not consider the feedback of the magnetic on the fluid through the Lorentz force. Finally, a major change came from the field of helioseismology, the measurements of the internal rotation profile of the Sun dramatically differed from theoretical expectations based on mean-field modelling. Even more crucially these measurements revealed the existence of the tachocline, a thin layer of strong shear located at the interface between the inner radiative core and the outer convective zone.

A number of subsequent studies have tried to overcome these issues in the framework of mean-field $\alpha\Omega$ modelling. In particular, flux transport dynamo models – based on a Babcock-Leighton generation mechanism – attribute an important role to meridional circulation (Choudhuri et al. 1995; Dikpati and Charbonneau 1999); on their side interface dynamo models assume that the α- and Ω-effects are spatially segregated on either sides of the core-envelope interface (Parker 1993; Charbonneau and MacGregor 1997). These studies attribute a crucial to the solar tachocline as being a place where toroidal fields can be strongly amplified up to the field strength required to explain sunspot properties and on timescales compatible with the solar cycle length. In parallel, the constantly-increasing computing capabilities have allowed to perform direct numerical simulations of dynamo action in spherical shells at high resolution. These simulations resolve the full set of equations that self-consistently describe the temporal evolution of the velocity and magnetic field, but are limited to regimes of parameters quite remote from real astrophysical objects. With numerical simulations, the interplay between differential rotation and magnetic fields can be studied (*e.g.,* Brown et al. 2010); the presence of a stratified layer that mimics the tachocline appears to facilitate the building of strong large-scale toroidal fields (Browning et al. 2006) though it is not essential (Brown et al. 2010); and cyclic polarity reversal start being observed (Käpylä et al. 2010; Brown et al. 2011). It is also worth noting that mean-field formalism remains a very useful tool to understand the magnetic field generation in numerical simulation (Schrinner et al. 2007).

3   Direct methods for magnetic field measurements

3.1   Zeeman effect

Direct measurements of stellar magnetic fields at the photospheric level rely on the properties of the Zeeman effect. This effect of the presence of a magnetic field on the formation of spectral lines has two aspects, represented on Fig. 2:

- A single spectral line splits into several components. In the case of the so-called normal Zeeman triplet three components are observable: a π component lying at the same wavelength as the null-field line, and two σ components shifted towards the red and the blue by an equal amount. The amount of π-to-σ splitting in a given spectral line is proportional to the modulus of the magnetic field B, in the CGS unit system it is given by:

$$\Delta\lambda_B = \frac{\lambda_0^2 e\, g_{\text{eff}} B}{4\pi m_e c^2} = 4.67 \times 10^{-12}\, \lambda_0^2\, g_{\text{eff}} B, \tag{3.1}$$

  where B is expressed in Gauss, λ_0 is the central wavelength of the line without magnetic field (in nm), and the effective Landé factor g_{eff} is a dimensionless number that quantities the sensitivity of a given line to the Zeeman effect. Spectral lines which are considered "magnetically sensitive" have Landé factors of the order of 1, up to a few units.

- The three components of the Zeeman-split spectral line have different polarization properties, the observed polarization depends on the relative orientation of the vector magnetic field with the line-of-sight of the observer. Stokes V (circular polarization) is sensitive to the line-of-sight component of the field (longitudinal field), whereas Q and U (linear) are sensitive to the component lying in the plane perpendicular to it.

In principle, from a measurement of all four Stokes parameters one can recover the magnetic field vector. Such an inversion procedure requires to solve the equations of polarised radiative transfer. The simplest solution is the so-called weak-field approximation which is valid if the Zeeman splitting $\Delta\lambda_B$ is small compared to the Doppler broadening of the line, in this case the individual π and σ components are not resolved, and in unpolarized light the Zeeman effect results in line broadening rather than splitting. In this case polarisation in spectral line is a 1st (circular) or 2nd (linear) order effect and the corresponding amplitudes are small compared to the unpolarised line depth:

$$\begin{cases} Q(\lambda) = -\dfrac{1}{4}g_{\text{eff}}^2 \Delta\lambda_B^2 \sin^2\theta \cos 2\chi \dfrac{d^2 I_0}{d\lambda^2} \\[2mm] U(\lambda) = -\dfrac{1}{4}g_{\text{eff}}^2 \Delta\lambda_B^2 \sin^2\theta \sin 2\chi \dfrac{d^2 I_0}{d\lambda^2} \\[2mm] V(\lambda) = -g_{\text{eff}} \Delta\lambda_B \cos\theta \dfrac{dI_0}{d\lambda} \end{cases}, \tag{3.2}$$

where I_0 is the corresponding Stokes I line profile without a magnetic field and the angles θ and χ are defined in Fig. 3. A more accurate description can be obtained
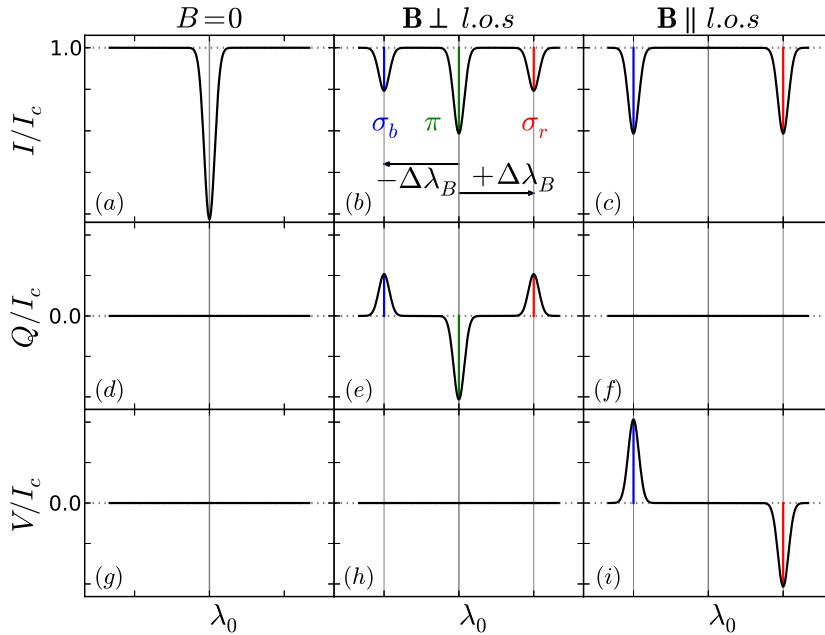
Figure 2: Schematic view of the Zeeman effect for a normal Zeeman triplet and a large splitting. The rows show from top to bottom the Stokes parameters I (intensity), Q (linear polarisation) and V (circular polarisation) normalized to the unpolarized continuum I_c (see Appendix B). Columns show from left to right the null-field case, and two magnetic cases with **B** perpendicular and parallel to the observer's line of sight. In the middle and right columns, the π, σ_b and σ_r components are respectively marked with a green, blue and red vertical line. The scale is the same for all panels. The x-axis ticks are in units of Zeeman splitting $\Delta\lambda_B$ (Eq. 3.1), and λ_0 is the central wavelength of the line without a magnetic field. The reference level (1 for I, 0 for Q, V) is plotted as a dotted gray line in each panel. The actual sign of Q and V depends on the polarity of the field.

with the analytical Unno-Rachkovsky solution (Unno 1956; Rachkovsky 1969) or by numerical solving. For a more detailed view of the Zeeman effect and other polarizing mechanisms in astrophysics, as well as an introduction to polarized radiative transfer, and spectropolarimetry the reader is referred to Landi Degl'Innocenti (1992), del Toro Iniesta (2003) and Landstreet (2009a,b,c).

3.2   Unpolarized spectroscopy

Since for a given field strength, the Zeeman splitting relative to the line wavelength is $\frac{\Delta\lambda_B}{\lambda_0} \propto \lambda_0\, g_{\text{eff}}$, such measurements are generally performed in high-Landé factor lines located in the red or even infrared part of stellar spectra. Let's consider
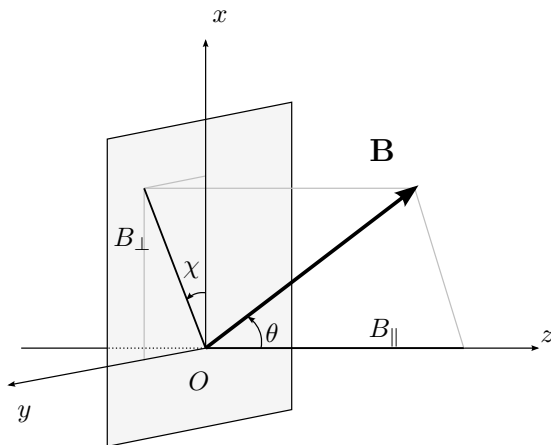
Figure 3: Geometry of the magnetic field vector with respect to the observer's line of sight (LoS) for the description of the Stokes parameters. The LoS is along the axis Oz. The plane xOy is perpendicular to it, with Ox the reference direction of the linear polarisation (see Appendix B). Measurements in circular polarisation (Stokes V) are sensitive to the longitudinal magnetic field $B_\parallel = B\cos\theta$. Measurements in linear polarisation (Q and U) are sensitive to the transversal component $B_\perp = B\sin\theta$.

the effect of a magnetic field of 2 kG (typical for a sunspot) in the favourable case of the Fe I line at 630.25 nm which has $g_{\rm eff} = 2.5$. The resulting splitting is $\Delta\lambda_B = 9.2 \times 10^{-3}$ nm, corresponding to a spectral resolution of $\frac{\lambda_0}{\Delta\lambda_B} = 6.8 \times 10^5$ or a velocity of 4.4 km s^{-1}. This can be directly observed on sunspots. However, for unresolved stars, spectra correspond to light integrated over the whole visible disc which likely features a distribution of magnetic field strengths and velocities. In addition, most active stars rotate with $v\sin i$ of a least a few km s^{-1}, further "blurring" the Zeeman splitting. Therefore the individual π and σ components are generally not observable[7], rather the Zeeman effect generally results in spectral line broadening. In order to disentangle between the effect of the magnetic field and other sources of broadening it is necessary to observe spectral lines of the same element with both low and high Landé factors and/or to observe both an active (to be studied) and an inactive (as a reference) star as similar as possible (temperature, gravity, metallicity). Most models consider that magnetic regions with assumed homogeneous field modulus B, cover a fraction f of the stellar surface, (Robinson 1980; Saar 1988); or even a range of local field strengths with

---

[7]Among non-degenerate stars, resolved π and σ components of Zeeman-split lines can be observed mostly in chemically peculiar Ap/Bp stars (which host fields of up to several tens of kG) (*e.g.,* Mathys et al. 1997).

each a different filling factor (Johns-Krull et al. 1999). The multiple parameters can generally not be constrained individually, the measured quantity is termed Bf, the product of the field modulus B in magnetic regions (assumed homogeneous) times the corresponding filling factor f, this quantity is sometimes called "magnetic flux" (although it is expressed in Gauss and not Maxwell) and reflects the magnetic field modulus averaged over the visible stellar disc.

M dwarfs are potentially good targets for magnetic field measurements since a significant fraction of them is very active (see lecture notes by X. Bonfils, this book), and their spectral energy distributions peak in the red or infrared where the Zeeman effect is stronger. Measurements based on atomic lines are possible for early and mid M dwarfs, however toward late spectral types molecular lines becomes more prominent (see chapter by F. Allard, this book) and further restrict the number of unblended atomic lines available for field measurements. The Wing-Ford band of FeH at 0.99 μm is composed of many lines spanning a range of Landé factors and is present through the whole M spectral type, making it an ideal candidate for magnetic field investigations in low-mass stars (Valenti and Johns-Krull 2001). To overcome the lack Landé factor values for these lines, Reiners and Basri (2006) have proposed an approach consisting of fitting a stellar spectra in the FeH region as a linear combination of the spectrum of an inactive star and a very active star (corrected for FeH band strength and $v \sin i$) for which the magnetic field modulus has been derived from the analysis of atomic lines. This method has been successfully applied to tens of stars spanning the whole M dwarf spectral type, and allowed to derive both $v \sin i$ and Bf with respective typical accuracies of 1 km s^{-1} and 0.5–1 kG. Future progress will likely come from theoretical computation of the Landé factors (Shulyak et al. 2010) as well as experimental determinations.

3.3 Spectropolarimetry

Spectropolarimetry consists in measuring at least one of the Stokes parameters Q, U, V as a function of wavelength, in addition to the unpolarized intensity spectrum I. Stokes V signatures in spectral lines have typical amplitudes of a few 10^{-3} of the level of the unpolarized continuum for active cool stars, Stokes Q and U are typically an order of magnitude smaller[8] (see Kochukhov et al. 2011, for full Stokes polarimetry of cool stars). Hence spectropolarimetric measurement require a very high polarimetric accuracy (in particular the acquisition and reduction procedures must ensure that instrumental polarisation is efficiently reduced, see *e.g.,* Donati et al. 1997), and spectra with high signal to noise ratio (SNR). This difficulty can be overcome to some extent with multi-line techniques which extract the polarimetric information from a large number of lines available in stellar spectra in order to compute an average profile with increased SNR. The achieved SNR multiplex gain can be as high as several tens when thousands of lines are used. Although some information is lost in the averaging process,

---

[8]In the weak-field approximation (Eq. 3.2), circular polarization (Stokes V) is a first order effect, whereas linear polarization (Stokes Q and U) is a second-order effect.
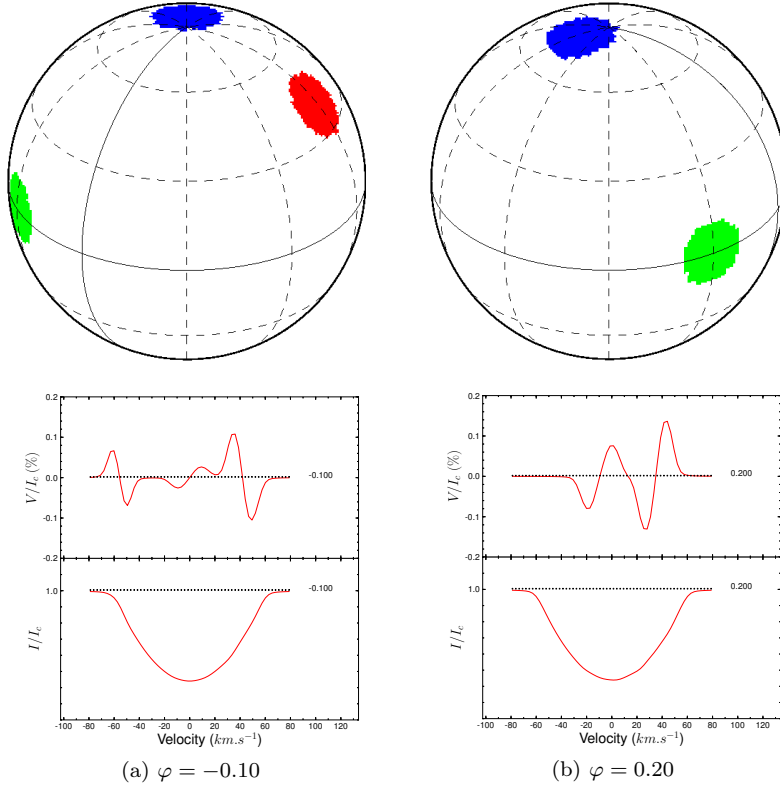
(a) $\varphi = -0.10$ (b) $\varphi = 0.20$

Figure 4: The principles of Zeeman-Doppler Imaging (ZDI). The favourable case of a rapidly rotating star ($v \sin i = 60$ km s^{-1}) for which the inclination of the rotation axis with respect to the line of sight (LoS) is $i = 60°$, is considered. Three magnetic spots with $B = 4$ kG cover each 1 % of the stellar surface. From left to right in panel (a) the orientation of **B** is azimuthal prograde (green), radial inward (blue) and radial outward (red). The Stokes I and V spectra are computed for a typical magnetically sensitive line using the Unno-Rachkovsky solution of the polarised radiative transfer equations taking into account radial velocity shifts and limb darkening, and convolved with an instrumental profile corresponding to $R = 60,000$. The star and the spectra are shown at two different epochs separated by 0.3 stellar rotation. The main effects on which ZDI relies are well visible: *(i)* the 3 magnetic spots are well separated in radial velocity space, and hence they produce well-separated signatures in the Stokes V line profile. *(ii)* Due to different angles of **B** with the LoS and limb angles, the 3 spots result in signatures with different Stokes V amplitudes although $B = 4$ kG for all of them; and for a given spot the amplitude depends on the rotational phase. *(iii)* The high-latitude spot is always visible and always contribute to the center of the line (low values of radial velocity), whereas low-latitude spots are visible during a fraction of the stellar rotational cycle and the corresponding Stokes V signatures cross most of the line profile width. *(iv)* The Stokes V signatures corresponding to the radial field spots keep a constant sign during stellar rotation, whereas for azimuthal field the signature reverses since the sign of the LoS projection of **B** changes sign.

this technique has the advantage of minimizing the effect of blends which can be considered as a random noise. Least squares deconvolution (hereafter LSD) is a widely used multi-line technique similar to the cross-correlation techniques used for accurate radial velocity measurements (Donati et al. 1997). LSD Stokes V profiles can be analyzed as a real spectral line with a reasonable accuracy for field strengths below 5 kG (Kochukhov et al. 2010) such as those encountered at the surface of low-mass stars. Alternative multi-line methods that can be superior to LSD in some respects are being developed (*e.g.,* Martínez González et al. 2008; Sennhauser and Berdyugina 2010).

The most easily derived magnetic quantity from spectropolarimetric data is the longitudinal field B_ℓ — *i.e.* the line-of-sight component of the magnetic field integrated over the visible stellar disc — which is related to Stokes I and V through:

$$B_\ell(\mathrm{G}) = -2.14 \times 10^{11} \frac{\displaystyle\int v\, V(v)\, \mathrm{d}v}{\lambda_0\, g_{\mathrm{eff}}\, c \displaystyle\int [I_c - I(v)]\, \mathrm{d}v}, \qquad (3.3)$$

where I_c is the unpolarised continuum, v is the radial velocity in the stellar rest frame, c is the speed of light in the same unit as v, λ_0 is the central wavelength of the line in nm, and g_{eff} is the effective Landé factor of the line (Rees and Semel 1979). However B_ℓ is an integral quantity which only reflects a limited fraction of the information contained in Stokes V line profiles. In order to take full advantage of high-resolution spectropolarimetric observations, these are often analyzed by means of Zeeman-Doppler Imaging (ZDI), a method introduced by Semel (1989) (and analogous to Doppler Imaging, see *e.g.,* Vogt et al. 1987) and continuously developed over the years (*e.g.,* Piskunov and Kochukhov 2002; Donati et al. 2006). ZDI relies on three effects which result in a strong relationship between the distribution of magnetic fields at the surface of a star and the temporal evolution of polarised signatures in spectral lines, as shown on Fig. 4. *(i)* Due to the Doppler effect induced by stellar rotation magnetic regions located at different projected distances from the rotation axis contribute to different parts of a rotationally broadened spectral line. *(ii)* Different parts of the star are visible under varying limb angles as the stars rotates. *(iii)* Zeeman-induced polarization in spectral lines is sensitive to the orientation of the magnetic field vector (see Sec. 3.1). ZDI is an inverse problem which is solved iteratively by comparing the times-series of polarized spectra computed from a model magnetic map with the observed one until convergence is reached. As there is no unique solution to this problem, a regularization scheme has to be used. The maximum entropy solution corresponding to lowest magnetic energy content is often used. ZDI studies of cool stars rely on Stokes V alone, Stokes Q and U are not observed due to their lower amplitudes. Donati and Brown (1997) have shown in the case of a dipolar field that a reliable ZDI reconstruction could be performed from Stokes V alone.
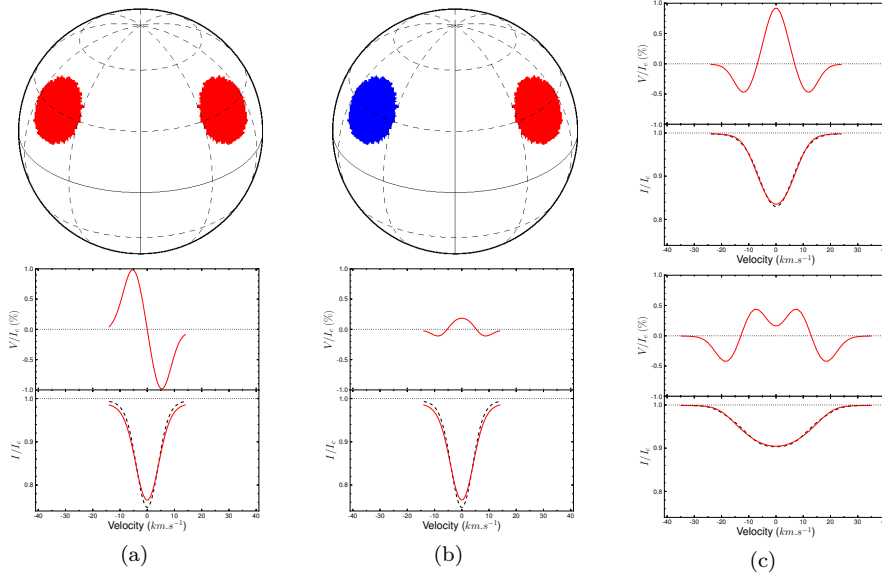
Figure 5: Stokes I and V spectra are computed as in Fig. 4 for two basic magnetic field distributions. In each Stokes I panel the black dashed line represents the corresponding spectral line without magnetic field. *(a)* Two magnetic spots with $B = 4$ kG cover each 1 % of the stellar surface, the field lines are radial and directed outward. *(b)* Same as *(a)* but the two spots have opposite polarities: in the left spot (blue) **B** is radial inward. In panels *(a)* and *(b)*, $v \sin i = 1$ km s^{-1}. The two magnetic field distributions cannot be distinguished from Stokes I measurements and are thus equally well detected. The two configurations are clearly distinguished from Stokes V measurements, although in case *(b)* the low amplitude of circular polarisation makes it more difficult to detect. *(c)* Same as *(b)* except for $v \sin i = 10$ km s^{-1} (top) and 20 km s^{-1} (bottom). For higher values of $v \sin i$ the contributions of the two spots are more easily separated in Stokes V spectra, whereas the Stokes I line broadening becomes harder to detect.

3.4   Comparison of the two approaches

From measurements of the Zeeman broadening of spectral lines in unpolarized light the disc-averaged magnetic field modulus can be estimated irrespective of the field complexity. The accuracy of the technique is limited by the fact that the Zeeman effect has to be disentangled from other sources of broadening and that the reference null-field profile with respect to which broadening is estimated is only known with a limited accuracy. With spectropolarimetry an information on the vector properties of the magnetic field is available, but tangled small-scale fields remain undetected. As opposed to Zeeman broadening measurements, the

null-field profile is perfectly known – null circular and linear polarization in spectral lines. Very weak longitudinal fields below 1 G can be measured from LSD Stokes V spectra provided the SNR is high enough (*e.g.,* Aurière et al. 2009). Measurements of Zeeman broadening in unpolarised light and spectropolarimetry provide complementary information on stellar magnetic fields. However it is not always possible to obtain both measurements for a given object: spectropolarimetric measurements are optimally performed for $v \sin i$ values of a few tens of $\mathrm{km\,s^{-1}}$ — which offer a good compromise between disentangling of magnetic regions of opposite polarities and line depth — whereas line broadening measurements are limited to approximately $v \sin i < 20\ \mathrm{km\,s^{-1}}$. In addition, both methods are affected by temperature inhomogeneities which can "hide" magnetic flux.

4   The fully convective transition

4.1   Magnetic fields of partly convective stars

Activity phenomena are observed on most cool stars. They are found to be variable or even to exhibit solar-like cycles in a number of cases (see chapter by X. Bonfils, this book). Surface magnetic fields are directly detected for a number of partly convective stars. Generation of magnetic fields in these partly-convective Sun-like stars is believed to rely on similar processes as in the Sun, with an important role of differential rotation ($\alpha\Omega$-type dynamo) and of the tachocline. In spite of the wide variety of stellar parameters ($0.35 < M_\star < 1.3\ \mathrm{M_\odot}$ considering only main sequence objects, rotation periods and activity levels spanning several orders of magnitude) these stars have a similar internal structure with an inner radiative zone, a convective envelope, and likely a tachocline in between. In addition, activity levels (expressed as luminosity in *e.g.,* X-rays or in the Hα line normalized to the stellar bolometric luminosity) of cool stars appear to be affected in the same way by rotation when it is expressed through the Rossby number Ro which measures the ratio of inertia to the Coriolis force or equivalently the ratio of the dynamical to rotational timescales [9] (*e.g.,* Mangeney and Praderie 1984; Noyes et al. 1984; Pizzolato et al. 2003).

Studies of partly-convective stars in unpolarised light have reported average magnetic fields from the detection threshold (a few hundred Gauss typically) up to several kG (*e.g.,* Saar 1996; Anderson et al. 2010). From these measurements, Saar (2001) have found a good correlation between Rossby number and magnetic flux ($Bf \propto Ro^{-1.2}$). Studies based on spectropolarimetric observations and Zeeman-Doppler Imaging have concluded that the larges-scale component of the field is dominated by the dipole and quadrupole modes for slow rotators, as is

---

[9]The Rossby number is defined as: Ro $= \frac{u_0}{\Omega L}$ or Ro$= \frac{P_{\mathrm{rot}}}{\tau_c}$, where u_0 is the typical fluid velocity, Ω the rotation rate, L a characteristic lengthscale (*e.g.,* the pressure scale height), P_{rot} the rotation period, and τ_c the convective turnover time. It is a local quantity that is expected to strongly depend on the radial coordinate inside the star. In observational stellar physics a global or empirical Rossby number is often used, in order to assign a unique number to a star.

observed on the Sun. For faster rotators higher order multipoles are predominant and a strong toroidal component is detected at the photospheric level (*e.g.,* Petit et al. 2008) — whereas on the Sun strong toroidal fields are thought to reside deep in the interior, mostly in the tachocline. A few polarity reversals or even full magnetic cycles have also been observed with these techniques, suggesting that fast rotators undergo faster magnetic cycles, although the dependence on stellar mass is not yet clear (*e.g.,* Fares et al. 2009; Morgenthaler et al. 2011).

4.2   Dynamo models of fully convective stars

Main sequence stars with masses below ~ 0.35 M$_\odot$ (*e.g.,* Chabrier and Baraffe 1997) or young solar-type stars (T Tauri stars, see *e.g.,* Siess et al. 2000) are fully convective (see Fig. 1) and therefore do not possess a tachocline. If this region is really a key element of the solar dynamo, fully convective stars should generate their magnetic fields by non-solar processes. This led theoreticians to model magnetic field generation in fully convective stars without an Ω-effect. Durney et al. (1993) first proposed that in these objects magnetic fields could be generated by a small-scale dynamo *i.e.* producing magnetic field at the scale of the fluid motions. Küker and Rüdiger (1999) and Chabrier and Küker (2006) performed mean-field modeling of brown dwarfs and fully convective stars, the α^2 dynamo resulted in steady (*i.e.* showing no reversal) non-axisymmetric field dominated by high order multipoles. Dynamo action in fully-convective stars has also been investigated with direct numerical simulations by Dobler et al. (2006) and Browning (2008). In these studies, such objects can generate strong and steady magnetic fields possessing a significant axisymmetric component. In addition Browning (2008) shows that in his simulations Maxwell stresses result in a very low level of differential rotation.

4.3   Magnetic fields of fully convective stars in unpolarised spectroscopy

Magnetic fields of main sequence M dwarfs have been investigated since the 1980s in unpolarised spectroscopy, using atomic lines (Saar and Linsky 1985; Saar 1994; Johns-Krull and Valenti 1996; Kochukhov et al. 2009). However, most *Bf* values now available have been obtained since Reiners and Basri (2006) have proposed a method to perform such measurements based on spectral lines of the FeH molecule (see Sec. 3.2). Measurements performed on stars located close to the fully convective limit are presented in Reiners and Basri (2007, 2009); Reiners et al. (2009a). Measured *Bf* values are plotted as a function of spectral type on Fig. 6a, they span the range 0–4 kG. No strong break can detected at the spectral type at which stars become fully convective (M3–M4), similarly to what is observed for activity proxies (in particular for X-ray and Hα emission, see chapter by X. Bonfils, this book). *(i)* The range of magnetic fluxes measured is similar to more massive solar-type stars. *(ii)* The observed scatter can be accounted for by the effect of rotation, there is evidence for a dependence on Rossby number similar to that observed for solar-type stars for stars of spectral type M0–M6 (see Reiners et al.
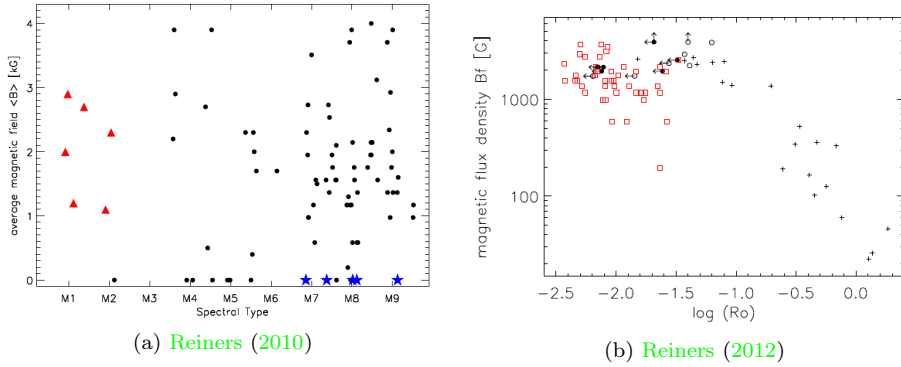
(a) Reiners (2010)   (b) Reiners (2012)

Figure 6: *(a)* Average magnetic fields of M dwarfs measured from Stokes I as a function of spectral type. Young early M dwarfs are depicted as red triangles, field M dwarfs as black circles and young accreting brown dwarfs as blue stars.*(b)* Average magnetic fields of G–K–M dwarfs derived from Stokes I measurements as a function of Rossby number. Crosses are Sun-like stars (Saar 1996, 2001), circles are M-type of spectral class M6 and earlier (Reiners et al. 2009a). For the latter, no period measurements are available and Rossby numbers are upper limits (they may shift to the left hand side in the figure). The black crosses and circles follow the rotation-activity relation known from activity indicators. Red squares are objects of spectral type M7–M9 (Reiners and Basri 2010) that do not seem to follow this trend ($\tau_c = 70$ dwas assumed for this sample).

2009a, and Fig. 6b): *Bf* increases towards low Ro, and then reaches a saturation level ($Bf \sim 2 - 4$ kG) for Ro~ 0.1 (*i.e.* $P_{\rm rot} \sim 6$ d for a M3 dwarf).

4.4   *Magnetic fields of fully convective stars in spectropolarimetry*

Following the first detection in polarised light of a large-scale magnetic field on a fully convective star by Donati et al. (2006), a spectropolarimetric survey of a small sample of active M dwarfs lying on both sides of the fully convective boundary has been carried out. The main results of this study are presented on Fig. 7, showing the main properties of the large-scale magnetic fields reconstructed with ZDI as a function of stellar mass and rotation period. A sharp change is observed close to the boundary to full-convection (Morin et al. 2008a,b; Donati et al. 2008b; Phan-Bao et al. 2009):

- M dwarfs more massive than ~ 0.5 M$_\odot$ (partly convective) exhibit large-scale magnetic fields with a strong toroidal component, even dominant in some cases; the poloidal component is strongly non-axisymmetric. For most of these stars, surface differential rotation can be derived, values are comprised
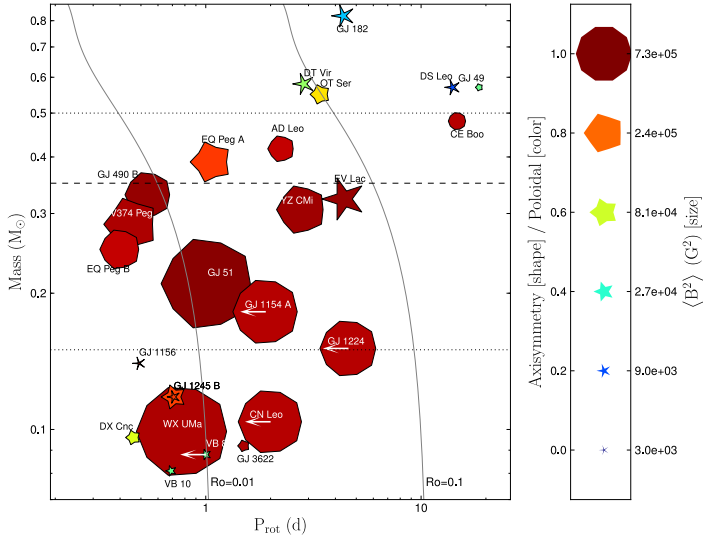
Figure 7: Properties of the large-scale magnetic fields of the sample of M dwarfs observed in spectropolarimetry as a function of rotation period and mass. Larger symbols indicate stronger fields, symbol shapes depict the degree of axisymmetry of the reconstructed magnetic field (from decagons for purely axisymmetric to sharp stars for purely non axisymmetric), and colours the field configuration (from blue for purely toroidal to red for purely poloidal). Solid lines represent contours of constant Rossby number $Ro = 0.1$ (saturation threshold) and 0.01. The theoretical full-convection limit ($M_\star \sim 0.35\,\mathrm{M_\odot}$) is plotted as a horizontal dashed line, and the approximate limits of the three stellar groups discussed in the text are represented as horizontal solid lines. White arrows mark stars for which only an upper limit for the rotation period is known. In these cases the field geometry is assumed, and the magnetic energy extrapolated from the longitudinal field values. Adapted from Morin et al. (2010).

between once and twice the solar rate approximately, and the magnetic fields evolve beyond recognition on a timescale of a few months. These properties are reminiscent of the observations of more massive (G and K) active stars (*cf.* Sec. 4.1).

- Stars with masses between ~ 0.2 and $0.5\,\mathrm{M_\odot}$ (close the fully convective limit) host much stronger large-scale magnetic field with radically different geometries: almost purely poloidal, generally nearly axisymmetric, always close to a dipole more or less tilted with respect to the rotation axis. These magnetic field distributions are observed to be stable on timescales of several years, and differential rotation (when measurable) is of the order or a tenth of the

solar rate. These findings are in partial agreement with the recent numerical study by Browning (2008). Similarly, it is observed that fully convective stars can generate strong and long-lived large-scale magnetic fields featuring a strong axisymmetric component, that are able to quench differential rotation. But almost purely poloidal surface magnetic fields are reported, whereas in the simulation the axisymmetric component of the field is mainly toroidal (although the simulation does not encompass the stellar surface).

- Much stronger large-scale magnetic fields are measured from Stokes V spectra for fully-convective stars with respect to partly-convective ones, whereas the typical Bf value derived from unpolarised measurement does not seem to be affected by the fully-convective transition. Hence the ratio of the magnetic fluxes recovered from Stokes V to the one recovered from I increases across the fully-convective boundary. This has been interpreted as evidence that magnetic fields of fully convective stars are organized on larger spatial scales than that of partly-convective ones.

It is worth noting that the sample does not allow to definitely disentangle the effects of mass and rotation on stellar magnetic fields. Further observations are needed to address this issue.

5 Very low mass stars and brown dwarfs

5.1 Dynamo models of ultracool dwarfs

Except for the energy production mechanism, late M and early L brown dwarfs are similar to very-low-mass stars: they are fully-convective objects with a highly conducting interior and are expected to sustain dynamo action in a similar way as fully-convective stars do (Chabrier and Küker 2006). However, two important differences between these ultracool dwarfs and fully-convective mid M dwarfs exist. *(i)* In ultracool dwarfs an outer layer with low electric conductivity is present at the surface. Mohanty et al. (2002) have shown that this layer could prevent the generation of magnetic stresses that are required to sustain a chromosphere. A decrease of the activity level measured in the Hα line has indeed been measured, as well as in X-rays (see chapter by X. Bonfils, this book). However radio luminosity remains at a high level McLean et al. (2012), in agreement with the mean-field modelling by Chabrier and Küker (2006) who conclude that the generation of magnetic fields through large-scale dynamo action should still be efficient in ultracool dwarfs. *(ii)* In a significant fraction of ultracool dwarfs dynamo likely operate in a very low Rossby number regime, *i.e.* strongly dominated by rotation. Indeed rotational braking appears to be very inefficient in these objects, with $v \sin i > 10$ km s^{-1} (*i.e.* $P_{\rm rot} < 0.5$ d) often measured (Reiners and Basri 2010; McLean et al. 2012); and convective turnover times are expected to be longer than in hotter objects from models (Chabrier and Küker 2006) as well as from observations of activity (Kiraga and Stepien 2007).

5.2   Magnetic fields of ultracool dwarfs in unpolarised light

Zeeman-induced broadening of spectral lines in ultracool dwarfs has so far only been investigated from molecular lines of FeH. Reiners and Basri (2010) present the analysis of rotation, magnetic field and activity of a volume-limited sample ($d < 20$ pc) of M7–M9.5 dwarfs. Strong magnetic fields (up to 4 kG) are detected down to the lowest temperatures probed (see Fig. 6a). However, as opposed to M0–M6 dwarfs discussed in Sec. 4.3, a number of stars rotating faster than 10 km s^{-1} ($\log Ro \lesssim -1.5$) exhibit average magnetic of the order of 1 kG (see Fig. 6b). This observation is interpreted as a breakdown of the magnetic field saturation at low Rossby numbers for ultracool dwarfs. Among 4 young accreting brown dwarfs with similar spectral types, Reiners et al. (2009b) also found systematically weak magnetic fields (upper limits of a few hundred Gauss), much weaker than what has been measured for young accreting low-mass stars (Johns-Krull 2007). These observations have not yet been explained by theoretical models.

5.3   Magnetic fields of ultracool dwarfs in spectropolarimetry

Morin et al. (2010) have studied a small sample of mid-to-late M dwarfs, including 9 with $M_\odot < 0.15$ M$_\odot$ (mostly at spectral types M5–M6), using spectropolarimetry. For 5 stars a ZDI study could be performed. Two different types of magnetism are found: two stars possess a strong large-scale magnetic field, predominantly dipolar (similar to those described in Sec. 4.4); whereas for three stars the large-scale field is much weaker and complex. For the four remaining objects, the Stokes V signatures and derived B_ℓ values indicate that such a dichotomy also exists. This is all the more surprising that all these stars have very similar stellar parameters ($0.08 < M_\star < 0.15$ M$_\odot$ and $0.4 < P_{\rm rot} < 1.5$ d for stars for which a period measurement is available), see Fig. 7, bottom-left corner. Such a behaviour had not been foreseen, and it is not yet clear whether another parameter than mass and rotation (such as age) plays an important role in determining the magnetic topology of stars, or if two types of dynamo genuinely coexist in this range of parameters. The 6 stars hosting a weak and multipolar large-scale field have been studied by Reiners and Basri (2007) and Reiners et al. (2009a) who derived $Bf > 1$ kG for all of them. Hence the precise relationship between the two types of magnetism observed in spectropolarimetry and the fade of the rotation-dominated dynamo inferred from unpolarised spectroscopy (Sec. 5.2) is still unclear.

5.4   Activity–magnetic field relations in ultracool dwarfs

The various activity proxies appear to correlate reasonably well with each other, as well as with rotation and magnetic field strength for most cool stars (see lecture notes by X. Bonfils, this book). However, these correlations appear to partly breakdown at late M spectral types. As mentioned in Sec. 5.1, the growing neutrality of the outer atmosphere towards low temperatures seems to inhibit chromospheric emission (*e.g.,* Mohanty and Basri 2003). Reiners and Basri (2010) have shown that $L_{\rm H\alpha}/L_{bol}$ still correlates with the surface magnetic flux for ultracool dwarfs,
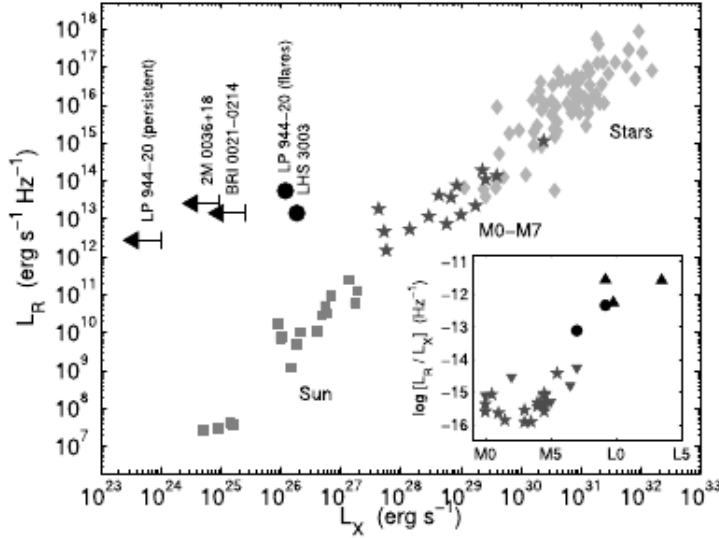
Figure 8: Radio luminosity as a function of X-ray luminosity for cool stars and solar flares. Both quantities correlate very well for spectral types earlier than M7. For later spectral types L_R remains almost constant whereas L_X drops. From Berger (2006).

although the correlation strongly depends on spectral type. As far as coronal emission is concerned, a remarkable correlation between X-ray and radio luminosities (respectively associated with thermal and non-thermal electron populations) exists for cool stars. This Güdel–Benz relation is valid over several order of magnitudes for quiescent and flaring integrated stellar luminosities as well as for solar flares (Guedel and Benz 1993; Benz and Guedel 1994). However it breaks down at spectral types later than M7: the observed X-ray luminosities (or upper limits) drop whereas radio luminosities remain at a roughly constant level for spectral types as late as mid L (see Fig. 8, and Berger 2006) and hence L_R/L_{bol} steeply increases towards late spectral types. The observations of polarised radio pulses at frequencies several GHz on a mid M dwarf and ultracool dwarfs have been interpreted as electron cyclotron maser instability emission (Hallinan et al. 2008), similar to what is detected on giant planets of the solar system (see *e.g.,* Zarka 1998). The observations are consistent with the present presence of a strong dipolar component of the magnetic field (polar fields of the order of one to a few kG) slightly tilted with respect to the rotation axis, in good agreement with spectropolarimetric observations (Hallinan et al. 2009; McLean et al. 2011).

6   Concluding remarks

6.1   A dynamo continuum low-mass stars, brown dwarfs, planets ?

The large-scale magnetic fields of a number of M dwarfs hosting a strong axial dipole component (see Sec. 4.4) are more reminiscent of the magnetic field of Jupiter rather than that of active solar-type stars. The parallel is further supported by theoretical studies: Goudard and Dormy (2008) have shown that a planetary dynamo simulation could switch from an Earth-like dipolar field to propagating dynamo waves reminiscent of the solar magnetic field simply by changing the aspect ratio of the convective region. Additionally, Christensen et al. (2009) showed that the scaling law between surface magnetic field strength and convective energy density initially derived by Christensen and Aubert (2006) from geodynamo simulations, can account for the observed field strengths of a number of objects including the Earth, Jupiter as well as rapidly rotating main sequence M dwarfs and young T Tauri stars. The concept of a dynamo continuum from planets to low-mass stars is already at the root of several studies (*e.g.,* Reiners and Christensen 2010; Morin et al. 2011; Schrinner et al. 2012) and will likely result in new advances in the forthcoming years.

6.2   Magnetic fields of young Suns

The focus of these notes has been mostly on main sequence M dwarfs. Young solar type stars (ages of a few Myr), called T Tauri stars, also undergo a fully convective phase. Strong magnetic fields are detected on these objects both in unpolarised spectroscopy (*e.g.,* Johns-Krull 2007) and in spectropolarimetry (*e.g.,* Donati et al. 2008a). It is likely that these objects generate their magnetic fields through dynamo processes similar to those acting in main sequence M dwarfs. This idea is further supported by the observation of a similar sequence of magnetic topologies from multipolar to dipolar towards thicker convection zones (relative to the stellar radius), and the possible existence of a domain where dipolar and multipolar fields coexist among T Tauri stars (Gregory, *et al.* 2012, submitted).

6.3   The need for combined observations

As evidenced throughout these notes, different approaches exist to study magnetism and activity in low-mass stars and brown dwarfs. Activity phenomena are indirect proxies, their relationships with magnetic fields rely on a complex physics and depends on stellar properties. Direct measurements based on the Zeeman effect allow us to directly probe the magnetic field at photospheric level. However such measurements based on unpolarised spectroscopy and spectropolarimetry provide us with different and complementary information that can generaly not be compared in a straightforward way, and have their own limitations. Much remains to be understood about the magnetism of low-mass stars, and even more for brown dwarfs. The ability to combine information stemming from different observational approaches is likely one of the ways towards future progress.

Appendix

A Poloidal and toroidal fields

A solenoidal (*i.e.* divergence-free) vector field can be decomposed uniquely into the sum of a poloidal and a toroidal components, according to:

$$\mathbf{B} = \mathbf{B}_{\mathrm{pol}} + \mathbf{B}_{\mathrm{tor}} = \nabla \times \nabla \times (P\mathbf{e_r}) + \nabla \times (T\mathbf{e_r}) \qquad (A.1)$$

In spherical coordinates, a poloidal field can have all 3 components non identically zero, whereas a toroidal vector field lies on a sphere *i.e.* it has no radial component. In the particular case of an axisymmetric vector field, $\mathbf{B}_{\mathrm{pol,axi}} = (B_r, B_\theta, 0)$ (no azimuthal component), whereas $\mathbf{B}_{\mathrm{tor,axi}} = (0, 0, B_\phi)$ (purely azimuthal). For such a solenoidal axisymmetric vector field, the poloidal–toroidal decomposition reads:

$$\mathbf{B}_{\mathrm{axi}} = \underbrace{\nabla \times (A\,\mathbf{e}_\phi)}_{\text{poloidal part}} + \underbrace{B\,\mathbf{e}_\phi}_{\text{toroidal part}} \qquad (A.2)$$

The reader is referred to Chandrasekhar (1961) for a more detailed explanation.

B Stokes parameters

Spectropolarimetry consists in studying the polarisation of a radiation (*i.e.* the temporal evolution of the electric and magnetic field vectors in the wavefront plane) as a function a wavelength. A complete description of an electromagnetic wave can be obtained with the four independent Stokes parameters:

- I is the unpolarised light intensity

- Q and U are the two orthogonal states which describe linear polarisation

- V measures the net circular polarisation.

These parameters can be simply defined from an idealized measurement procedure. Let's consider an ideal linear polarising filter and two ideal circular right- and left-handed polarising filters. We consider a incident radiation to be characterized, and a reference direction (in the wavefront plane) for the measurement of linear polarisation. We note I_{α° the intensity measured through perfect linear polarizer with a polarizing direction making an angle α with respect to the reference direction. $I_{\circlearrowright}$ and $I_{\circlearrowleft}$ represent the intensity measured through perfect circular polarizer selecting respectively right-hand and left-hand circular polarisation. I_{0°, $I_{45^\circ}, I_{90^\circ}, I_{135^\circ}, I_{\circlearrowright}$ and $I_{\circlearrowleft}$ are successively measured. The Stokes parameters are then defined as shown in Fig. 9, see also Landi Degl'Innocenti (1992).

Figure 9: Definition of the Stokes parameters from the measurement point of view according to the IAU (1973) convention. The notation I_{α° represents the intensity measured through perfect linear polarizer with a polarizing direction making an angle α with respect to a reference direction, taken to be the North–South, so that $+Q$ corresponds to a linear polarisation aligned with the North–South axis. $I_\circlearrowright$ and $I_\circlearrowleft$ represent the intensity measured through perfect circular polarizer selecting respectively right-handed and left-handed circular polarisation.

Acknowledgements

References

Anderson, R. I., Reiners, A., and Solanki, S. K.: 2010, *A&A* **522**, A81

Aurière, M., Wade, G. A., Konstantinova-Antova, R., Charbonnel, C., Catala, C., Weiss, W. W., Roudier, T., Petit, P., Donati, J.-F., Alecian, E., Cabanac, R., van Eck, S., Folsom, C. P., and Power, J.: 2009, *A&A* **504**, 231

Babcock, H. W.: 1961, *ApJ* **133**, 572

Babcock, H. W. and Babcock, H. D.: 1955, *ApJ* **121**, 349

Benz, A. O. and Guedel, M.: 1994, *A&A* **285**, 621

Berger, E.: 2006, *ApJ* **648**, 629

Bonfils, X., Delfosse, X., Udry, S., Forveille, T., Mayor, M., Perrier, C., Bouchy, F., Gillon, M., Lovis, C., Pepe, F., Queloz, D., Santos, N. C., Ségransan, D., and Bertaux, J.-L.: 2011, *ArXiv e-prints*

Bouvier, J.: 2009, in C. Neiner & J.-P. Zahn (ed.), *EAS Publications Series*, Vol. 39 of *EAS Publications Series*, pp 199–209

Bouvier, J., Alencar, S. H. P., Harries, T. J., Johns-Krull, C. M., and Romanova, M. M.: 2007, *Protostars and Planets V* pp 479–494

Braithwaite, J. and Spruit, H. C.: 2004, *Nature* **431**, 819

Brandenburg, A. and Subramanian, K.: 2005, *Phys. Rep.* **417**, 1

Brown, B. P., Browning, M. K., Brun, A. S., Miesch, M. S., and Toomre, J.: 2010, *ApJ* **711**, 424

Brown, B. P., Miesch, M. S., Browning, M. K., Brun, A. S., and Toomre, J.: 2011, *ApJ* **731**, 69

Browning, M. K.: 2008, *ApJ* **676**, 1262

Browning, M. K., Miesch, M. S., Brun, A. S., and Toomre, J.: 2006, *ApJ* **648**, L157

Chabrier, G. and Baraffe, I.: 1997, *A&A* **327**, 1039

Chabrier, G., Gallardo, J., and Baraffe, I.: 2007, *A&A* **472**, L17

Chabrier, G. and Küker, M.: 2006, *A&A* **446**, 1027

Chandrasekhar, S.: 1961, *Hydrodynamic and hydromagnetic stability*, International Series of Monographs on Physics, Oxford: Clarendon, 1961

Charbonneau, P.: 2010, *Living Reviews in Solar Physics* **7**, 3

Charbonneau, P. and MacGregor, K. B.: 1997, *ApJ* **486**, 502

Choudhuri, A. R., Schussler, M., and Dikpati, M.: 1995, *A&A* **303**, L29

Christensen, U. R. and Aubert, J.: 2006, *Geophysical Journal International* **166**, 97

Christensen, U. R., Holzwarth, V., and Reiners, A.: 2009, *Nature* **457**, 167

Cowling, T. G.: 1933, *MNRAS* **94**, 39

del Toro Iniesta, J. C.: 2003, *Introduction to Spectropolarimetry*

Dikpati, M. and Charbonneau, P.: 1999, *ApJ* **518**, 508

Dobler, W., Stix, M., and Brandenburg, A.: 2006, *ApJ* **638**, 336

Donati, J.-F. and Brown, S. F.: 1997, *A&A* **326**, 1135

Donati, J.-F., Howarth, I. D., Jardine, M. M., Petit, P., Catala, C., Landstreet, J. D., Bouret, J.-C., Alecian, E., Barnes, J. R., Forveille, T., Paletou, F., and Manset, N.: 2006, *MNRAS* **370**, 629

Donati, J.-F., Jardine, M. M., Gregory, S. G., Petit, P., Paletou, F., Bouvier, J., Dougados, C., Ménard, F., Cameron, A. C., Harries, T. J., Hussain, G. A. J., Unruh, Y., Morin, J., Marsden, S. C., Manset, N., Aurière, M., Catala, C., and Alecian, E.: 2008a, *MNRAS* **386**, 1234

Donati, J.-F. and Landstreet, J. D.: 2009, *ARA&A* **47**, 333

Donati, J.-F., Morin, J., Petit, P., Delfosse, X., Forveille, T., Aurière, M., Cabanac, R., Dintrans, B., Fares, R., Gastine, T., Jardine, M. M., Lignières, F., Paletou, F., Velez, J. C. R., and Théado, S.: 2008b, *MNRAS* **390**, 545

Donati, J.-F., Semel, M., Carter, B. D., Rees, D. E., and Collier Cameron, A.: 1997, *MNRAS* **291**, 658

Dorch, S. B. F. and Ludwig, H.-G.: 2002, *Astronomische Nachrichten* **323**, 402

Dormy, E. and Soward, A. M.: 2007, *Mathematical aspects of natural dynamos*

Durney, B. R., De Young, D. S., and Roxburgh, I. W.: 1993, *Sol. Phys.* **145**, 207

Elsasser, W. M.: 1946, *Phys. Rev.* **69**, 106

Fares, R., Donati, J.-F., Moutou, C., Bohlender, D., Catala, C., Deleuil, M., Shkolnik, E., Collier Cameron, A., Jardine, M. M., and Walker, G. A. H.: 2009, *MNRAS* **398**, 1383

Goudard, L. and Dormy, E.: 2008, *Europhysics Letters* **83**, 59001

Guedel, M. and Benz, A. O.: 1993, *ApJ* **405**, L63

Hale, G. E.: 1908, *ApJ* **28**, 315

Hale, G. E., Ellerman, F., Nicholson, S. B., and Joy, A. H.: 1919, *ApJ* **49**, 153

Hallinan, G., Antonova, A., Doyle, J. G., Bourke, S., Lane, C., and Golden, A.: 2008, *ApJ* **684**, 644

Hallinan, G., Doyle, G., Antonova, A., Bourke, S., Jardine, M., Donati, J.-F., Morin, J., and Golden, A.: 2009, in E. Stempels (ed.), *American Institute of Physics Conference Series*, Vol. 1094 of *American Institute of Physics Conference Series*, pp 146–151

IAU: 1973, *Transactions of the IAU*, Technical report

Irwin, J., Berta, Z. K., Burke, C. J., Charbonneau, D., Nutzman, P., West, A. A., and Falco, E. E.: 2011, *ApJ* **727**, 56

Johns-Krull, C. M.: 2007, *ApJ* **664**, 975

Johns-Krull, C. M. and Valenti, J. A.: 1996, *ApJ* **459**, L95

Johns-Krull, C. M., Valenti, J. A., and Koresko, C.: 1999, *ApJ* **516**, 900

Käpylä, P. J., Korpi, M. J., Brandenburg, A., Mitra, D., and Tavakol, R.: 2010, *Astronomische Nachrichten* **331**, 73

Kiraga, M. and Stepien, K.: 2007, *Acta Astronomica* **57**, 149

Kochukhov, O., Heiter, U., Piskunov, N., Ryde, N., Gustafsson, B., Bagnulo, S., and Plez, B.: 2009, in E. Stempels (ed.), *American Institute of Physics Conference Series*, Vol. 1094 of *American Institute of Physics Conference Series*, pp 124–129

Kochukhov, O., Makaganiuk, V., and Piskunov, N.: 2010, *A&A* **524**, A5

Kochukhov, O., Makaganiuk, V., Piskunov, N., Snik, F., Jeffers, S. V., Johns-Krull, C. M., Keller, C. U., Rodenhuis, M., and Valenti, J. A.: 2011, *ApJ* **732**, L19

Küker, M. and Rüdiger, G.: 1999, *A&A* **346**, 922

Landi Degl'Innocenti, E.: 1992, *Magnetic field measurements*, p. 71

Landstreet, J. D.: 2009a, in C. Neiner & J.-P. Zahn (ed.), *EAS Publications Series*, Vol. 39 of *EAS Publications Series*, pp 1–20

Landstreet, J. D.: 2009b, in C. Neiner & J.-P. Zahn (ed.), *EAS Publications Series*, Vol. 39 of *EAS Publications Series*, pp 21–37

Landstreet, J. D.: 2009c, in C. Neiner & J.-P. Zahn (ed.), *EAS Publications Series*, Vol. 39 of *EAS Publications Series*, pp 39–53

Larmor, J.: 1919, *Rep. Brit. Assoc. Adv. Sci.*

Leighton, R. B.: 1969, *ApJ* **156**, 1

Mangeney, A. and Praderie, F.: 1984, *A&A* **130**, 143

Martínez González, M. J., Asensio Ramos, A., Carroll, T. A., Kopf, M., Ramírez Vélez, J. C., and Semel, M.: 2008, *A&A* **486**, 637

Mathys, G., Hubrig, S., Landstreet, J. D., Lanz, T., and Manfroid, J.: 1997, *A&AS* **123**, 353

Maunder, E. W.: 1904, *MNRAS* **64**, 747

Mayor, M. and Queloz, D.: 1995, *Nature* **378**, 355

McLean, M., Berger, E., Irwin, J., Forbrich, J., and Reiners, A.: 2011, *ApJ* **741**, 27

McLean, M., Berger, E., and Reiners, A.: 2012, *ApJ* **746**, 23

Moffatt, H. K.: 1970, *Journal of Fluid Mechanics* **41**, 435

Mohanty, S. and Basri, G.: 2003, *ApJ* **583**, 451

Mohanty, S., Basri, G., Shu, F., Allard, F., and Chabrier, G.: 2002, *ApJ* **571**, 469

Morgenthaler, A., Petit, P., Morin, J., Aurière, M., Dintrans, B., Konstantinova-Antova, R., and Marsden, S.: 2011, *Astronomische Nachrichten* **332**, 866

Morin, J., Donati, J., Petit, P., Delfosse, X., Forveille, T., and Jardine, M. M.: 2010, *MNRAS* **407**, 2269

Morin, J., Donati, J.-F., Forveille, T., Delfosse, X., Dobler, W., Petit, P., Jardine, M. M., Cameron, A. C., Albert, L., Manset, N., Dintrans, B., Chabrier, G., and Valenti, J. A.: 2008a, *MNRAS* **384**, 77

Morin, J., Donati, J.-F., Petit, P., Delfosse, X., Forveille, T., Albert, L., Aurière, M., Cabanac, R., Dintrans, B., Fares, R., Gastine, T., Jardine, M. M., Lignières, F., Paletou, F., Ramirez Velez, J. C., and Théado, S.: 2008b, *MNRAS* **390**, 567

Morin, J., Dormy, E., Schrinner, M., and Donati, J.-F.: 2011, *MNRAS* **418**, L133

Noyes, R. W., Hartmann, L. W., Baliunas, S. L., Duncan, D. K., and Vaughan, A. H.: 1984, *ApJ* **279**, 763

Ossendrijver, M.: 2003, *A&A Rev.* **11**, 287

Parker, E. N.: 1955, *ApJ* **122**, 293

Parker, E. N.: 1975, *ApJ* **198**, 205

Parker, E. N.: 1993, *ApJ* **408**, 707

Petit, P., Dintrans, B., Solanki, S. K., Donati, J.-F., Aurière, M., Lignières, F., Morin, J., Paletou, F., Ramirez Velez, J., Catala, C., and Fares, R.: 2008, *MNRAS* **388**, 80

Phan-Bao, N., Lim, J., Donati, J.-F., Johns-Krull, C. M., and Martín, E. L.: 2009, *ApJ* **704**, 1721

Piskunov, N. and Kochukhov, O.: 2002, *A&A* **381**, 736

Pizzolato, N., Maggio, A., Micela, G., Sciortino, S., and Ventura, P.: 2003, *A&A* **397**, 147

Rachkovsky, D. N.: 1969, *Izvestiya Ordena Trudovogo Krasnogo Znameni Krymskoj Astrofizicheskoj Observatorii* **40**, 127

Rädler, K.-H. and Rheinhardt, M.: 2007, *Geophysical and Astrophysical Fluid Dynamics* **101**, 117

Rees, D. E. and Semel, M. D.: 1979, *A&A* **74**, 1

Reiners, A.: 2008, in S. Röser (ed.), *Reviews in Modern Astronomy*, Vol. 20 of *Reviews in Modern Astronomy*, p. 40

Reiners, A.: 2010, *ArXiv e-prints*

Reiners, A.: 2012, *Living Reviews in Solar Physics* **9**, 1

Reiners, A. and Basri, G.: 2006, *ApJ* **644**, 497

Reiners, A. and Basri, G.: 2007, *ApJ* **656**, 1121

Reiners, A. and Basri, G.: 2009, *A&A* **496**, 787

Reiners, A. and Basri, G.: 2010, *ApJ* **710**, 924

Reiners, A., Basri, G., and Browning, M.: 2009a, *ApJ* **692**, 538

Reiners, A., Basri, G., and Christensen, U. R.: 2009b, *ApJ* **697**, 373

Reiners, A. and Christensen, U. R.: 2010, *A&A* **522**, A13

Reiners, A. and Mohanty, S.: 2012, *ApJ* **746**, 43

Roberts, P. and Stix, M.: 1971, *The Turbulent Dynamo: A Translation of a Series of Papers by F. Krause, K.-H Radler, and M. Steenbeck*, Technical Report NCAR/TN-60+IA

Robinson, Jr., R. D.: 1980, *ApJ* **239**, 961

Rüdiger, G. and Hollerbach, R.: 2004, *The magnetic universe : geophysical and astrophysical dynamo theory*

Rüdiger, G., Kitchatinov, L. L., and Brandenburg, A.: 2011, *Sol. Phys.* **269**, 3

Saar, S. H.: 1988, *ApJ* **324**, 441

Saar, S. H.: 1994, in D. M. Rabin, J. T. Jefferies, & C. Lindsey (ed.), *Infrared Solar Physics*, Vol. 154 of *IAU Symposium*, p. 493

Saar, S. H.: 1996, in K. G. Strassmeier & J. L. Linsky (ed.), *Stellar Surface Structure*, Vol. 176 of *IAU Symposium*, p. 237

Saar, S. H.: 2001, in R. J. Garcia Lopez, R. Rebolo, & M. R. Zapaterio Osorio (ed.), *11th Cambridge Workshop on Cool Stars, Stellar Systems and the Sun*, Vol. 223 of *Astronomical Society of the Pacific Conference Series*, p. 292

Saar, S. H. and Linsky, J. L.: 1985, *ApJ* **299**, L47

Sanderson, T. R., Appourchaux, T., Hoeksema, J. T., and Harvey, K. L.: 2003, *Journal of Geophysical Research (Space Physics)* **108**, 1035

Schrinner, M., Petitdemange, L., and Dormy, E.: 2012, *ArXiv e-prints*

Schrinner, M., Rädler, K.-H., Schmitt, D., Rheinhardt, M., and Christensen, U. R.: 2007, *Geophysical and Astrophysical Fluid Dynamics* **101**, 81

Schwabe, M.: 1844, *Astronomische Nachrichten* **21**, 233

Semel, M.: 1989, *A&A* **225**, 456

Sennhauser, C. and Berdyugina, S. V.: 2010, *A&A* **522**, A57

Shulyak, D., Reiners, A., Wende, S., Kochukhov, O., Piskunov, N., and Seifahrt, A.: 2010, *A&A* **523**, A37

Siess, L., Dufour, E., and Forestini, M.: 2000, *A&A* **358**, 593

Solanki, S. K., Inhester, B., and Schüssler, M.: 2006, *Reports on Progress in Physics* **69**, 563

Spruit, H. C.: 2011, *Theories of the Solar Cycle: A Critical View*, p. 39

Steenbeck, M. and Krause, F.: 1969a, *Astronomische Nachrichten* **291**, 49

Steenbeck, M. and Krause, F.: 1969b, *Astronomische Nachrichten* **291**, 271

Steenbeck, M., Krause, F., and Rädler, K.-H.: 1966, *Zeitschrift Naturforschung Teil A* **21**, 369

Tsinganos, K., Ray, T., and Stute, M.: 2009, *Protostellar Jets in Context*

Unno, W.: 1956, *PASJ* **8**, 108

Valenti, J. A. and Johns-Krull, C.: 2001, in G. Mathys, S. K. Solanki, & D. T. Wickramasinghe (ed.), *Magnetic Fields Across the Hertzsprung-Russell Diagram*, Vol. 248 of *Astronomical Society of the Pacific Conference Series*, p. 179

Vögler, A. and Schüssler, M.: 2007, *A&A* **465**, L43

Vogt, S. S., Penrod, G. D., and Hatzes, A. P.: 1987, *ApJ* **321**, 496

Whelan, E. T., Ray, T. P., Bacciotti, F., Natta, A., Testi, L., and Randich, S.: 2005, *Nature* **435**, 652

Zarka, P.: 1998, *J. Geophys. Res.* **103**, 20159